Am J Physiol Endocrinol Metab 320: E938–E950, 2021.
First published April 5, 2021; doi:10.1152/ajpendo.00010.2021

american physiological society

AMERICAN JOURNAL OF PHYSIOLOGY
ENDOCRINOLOGY AND METABOLISM

RESEARCH ARTICLE

Genetically increasing flux through β-oxidation in skeletal muscle increases mitochondrial reductive stress and glucose intolerance

Cody D. Smith,[1,2] Chien-Te Lin,[1,2] Shawna L. McMillin,[1,3] Luke A. Weyrauch,[1,3] Cameron A. Schmidt,[1,2] Cheryl A. Smith,[1,2] Irwin J. Kurland,[5] Carol A. Witczak,[1,2,3,4] and P. Darrell Neufer[1,2,3,4]

[1]*East Carolina Diabetes and Obesity Institute, Brody School of Medicine, East Carolina University, Greenville, North Carolina;* [2]*Department of Physiology, Brody School of Medicine, East Carolina University, Greenville, North Carolina;* [3]*Department of Biochemistry & Molecular Biology, Brody School of Medicine, East Carolina University, Greenville, North Carolina;* [4]*Department of Kinesiology, East Carolina University, Greenville, North Carolina; and* [5]*Department of Medicine, Albert Einstein College of Medicine, Bronx, New York*

Abstract

Elevated mitochondrial hydrogen peroxide (H_2O_2) emission and an oxidative shift in cytosolic redox environment have been linked to high-fat-diet-induced insulin resistance in skeletal muscle. To test specifically whether increased flux through mitochondrial fatty acid oxidation, in the absence of elevated energy demand, directly alters mitochondrial function and redox state in muscle, two genetic models characterized by increased muscle β-oxidation flux were studied. In mice overexpressing peroxisome proliferator-activated receptor-α in muscle (MCK-PPARα), lipid-supported mitochondrial respiration, membrane potential ($\Delta\Psi_m$), and H_2O_2 production rate (JH_2O_2) were increased, which coincided with a more oxidized cytosolic redox environment, reduced muscle glucose uptake, and whole body glucose intolerance despite an increased rate of energy expenditure. Similar results were observed in lipin-1-deficient, fatty-liver dystrophic mice, another model characterized by increased β-oxidation flux and glucose intolerance. Crossing MCAT (mitochondria-targeted catalase) with MCK-PPARα mice normalized JH_2O_2 production, redox environment, and glucose tolerance, but surprisingly, both basal and absolute insulin-stimulated rates of glucose uptake in muscle remained depressed. Also surprising, when placed on a high-fat diet, MCK-PPARα mice were characterized by much lower whole body, fat, and lean mass as well as improved glucose tolerance relative to wild-type mice, providing additional evidence that overexpression of PPARα in muscle imposes more extensive metabolic stress than experienced by wild-type mice on a high-fat diet. Overall, the findings suggest that driving an increase in skeletal muscle fatty acid oxidation in the absence of metabolic demand imposes mitochondrial reductive stress and elicits multiple counterbalance metabolic responses in an attempt to restore bioenergetic homeostasis.

NEW & NOTEWORTHY Prior work has suggested that mitochondrial dysfunction is an underlying cause of insulin resistance in muscle because it limits fatty acid oxidation and therefore leads to the accumulation of cytotoxic lipid intermediates. The implication has been that therapeutic strategies to accelerate β-oxidation will be protective. The current study provides evidence that genetically increasing flux through β-oxidation in muscle imposes reductive stress that is not beneficial but rather detrimental to metabolic regulation.

fat oxidation; glucose tolerance; insulin resistance; mitochondria; skeletal muscle

INTRODUCTION

Cytosolic accumulation of lipid intermediates has long been associated with the development of insulin resistance in skeletal muscle and liver (1–3). Multiple lines of evidence have also shown that basal fatty acid oxidation rates (4) and the capacity of skeletal muscle to oxidize lipids (5) are lower in obese/diabetic humans. A number of additional studies using noninvasive magnetic resonance spectroscopy (MRS) have provided evidence that muscle mitochondrial function at rest and/or during recovery from exercise is lower in insulin-resistant elderly, obese diabetics, and insulin-resistant offspring of type 2 diabetics (6–9). Collectively, these findings led to the hypothesis that inherent or acquired mitochondrial dysfunction underlies the development of insulin resistance by diverting fatty acids away from oxidation and toward the synthesis and cytosolic accumulation of toxic lipid species (10, 11).

One of the implications of the mitochondrial dysfunction theory is that genetic or pharmacological approaches that stimulate an increase in fatty acid oxidation should prevent or reverse high-fat-diet-induced insulin resistance. Initial

Correspondence: P. D. Neufer (neuferp@ecu.edu).
Submitted 13 January 2021 / Revised 24 March 2021 / Accepted 26 March 2021

studies appeared to support this hypothesis, as mice lacking acetyl-CoA carboxylase 2 ($ACC2^{-/-}$), an enzyme normally involved in suppressing fatty acid entry into the mitochondria, were found to have higher whole body and muscle fatty acid oxidation rates and to be protected from high-fat-diet-induced insulin resistance (12–14). However, two subsequent ACC2 knockout models, one whole body (15) and one muscle specific (16), failed to replicate these findings. The discrepancy appears to be due to an unexplained increased rate of energy expenditure in the first model (14), a feature common to many other genetic models characterized by protection from high-fat-diet-induced obesity and insulin resistance (17–19).

Two other unique genetic models have been used to test the impact of increased skeletal muscle β-oxidation flux on insulin sensitivity, a muscle-specific peroxisome proliferator-activated receptor-α (MCK-PPARα)-overexpressing mouse and the lipin-1-deficient, fatty-liver dystrophic mouse (20–23). MCK-PPARα mice are characterized by enhanced expression of β-oxidation genes and increased muscle fatty acid oxidation rates, but instead of being protected from diet-induced insulin resistance, the mice develop glucose intolerance and insulin resistance even on a low-fat diet (20). Similar to MCK-PPARα mice, mice that are deficient in lipin-1, which is required for adipose differentiation, are characterized by enhanced expression of β-oxidation genes in skeletal muscle and increased reliance on fat oxidation but also develop glucose intolerance and insulin resistance (22, 24, 25). Interestingly, short-term inhibition of mitochondrial fatty acid oxidation improves glucose tolerance in MCK-PPARα mice despite a profound increase in intramuscular lipid content (20), implying that during high dietary fat intake, increased flux through β-oxidation rather than increased ectopic lipid accumulation is driving the glucose intolerance and insulin resistance.

From a bioenergetics perspective, an increase in fatty acid oxidation that is not driven by either an increase in energy expenditure or a decrease in carbohydrate oxidation should raise the redox free energy driving force (i.e., ΔG_{redox}) on the electron transport system (ETS), increasing the mitochondrial membrane potential ($\Delta\Psi_m$), reductive stress within the ETS, and, consequently, the rate of superoxide/hydrogen peroxide (JH_2O_2) production (26). Elevated mitochondrial JH_2O_2 emission has been linked to the etiology of high-fat-diet-induced insulin resistance (27–31). The purpose of the present study, therefore, was to test this hypothesis by using both the MCK-PPARα and lipin-1-deficient genetic models, as well as by crossing MCK-PPARα mice with mice overexpressing the H_2O_2 detoxifying enzyme catalase targeted specifically to mitochondria (MCAT) (32). Collectively, the findings support the contention that accelerating flux through β-oxidation, in-and-of-itself, imposes reductive stress that is multifactorial and detrimental to metabolic regulation at both the muscle and the whole body level.

EXPERIMENTAL PROCEDURES

Animal Use

Approval by the East Carolina University Institutional Animal Care and Use Committee was obtained before all animal studies. Transgenic mice overexpressing peroxisome proliferator-activated receptor-α [MCK-PPARα (20)] or mitochondria-targeted catalase [MCAT (32)], both initially on C57BL/6J background, were backcrossed 10+ generations to the full congenic C57BL/6NJ (B6N) strain. For some experiments, MCK-PPARα (B6N) and MCAT (B6N) mice were mated to produce MCK-PPARα/MCAT (B6N) double transgenics. BALB/cByJ^{-+}/*fld* mice were obtained from The Jackson Laboratory (Bar Harbor, ME) and bred to produce lipin-1-deficient (−/−) and wild-type (+/+ and +/−) mice. Lipin-1 heterozygous mice are indistinguishable from wild-type mice (23); as such, all comparisons were between lipin-1 (−/−) versus (+/−) mice. All mice were housed in a temperature-controlled (22°C) facility with a 12-h light/dark cycle. Only male mice between 3 and 5 mo of age were used for experiments. All mice were maintained on a low-fat (10% by kcal) diet (Research Diets D06041501), unless otherwise noted. One week before the study, body composition was determined on select cohorts of mice by magnetic resonance imaging (Echo MRI, Houston, TX), and whole body calorimetry (Phenomaster/Labmaster, TSE Systems, Chesterfield, MO) was performed for 48 h after a 48-h acclimatization period. At the conclusion of the diet intervention, mice were anesthetized and portions of the red (RG) and white (WG) gastrocnemius muscles were dissected for permeabilized muscle fiber bundle (PmFB) preparations. Soleus and/or extensor digitorum longus (EDL) muscles were dissected and pinned by the tendons at resting length for glucose uptake assays. Plantaris muscles were incubated with insulin to assess key glucometabolic proteins. Tibialis anterior (TA) and EDL were flash frozen in $N_{2(l)}$ for later analysis.

Glucose Tolerance Tests

Mice were fasted for 5–6 h before experimentation. Blood glucose was measured from the tail vein using the AlphaTrak 2 animal glucometer (Abbott laboratories) at time points 0, 15, 30, 60, and 90 min after intraperitoneal glucose injection [20% dextrose saline solution (Hospira Inc., Lake Forest, IL; 2.5 g/kg fat-free mass)]. Glucose tolerance was calculated from the area under the curve using the trapezoid rule after normalizing to fasting blood glucose levels.

^{3}H-2-Deoxyglucose Uptake Assay

For maximal insulin-stimulated glucose uptake, soleus and EDL muscles were incubated in continuously gassed (95% O_2, 5% CO_2), 37°C Krebs–Ringer bicarbonate (KRB) buffer containing 117 mM NaCl, 4.7 mM KCl, 2.5 mM $CaCl_2$, 1.2 mM KH_2PO_4, 1.2 mM $MgSO_4$, and 24.6 mM $NaHCO_3$ supplemented with 2 mM pyruvate for 40 min, followed by an additional 10 min in the presence or absence of maximal insulin (50 mU/mL, Sigma-Aldrich, Cat. No. 11376497001). To assess glucose uptake, muscles were incubated in continuously gassed, 37°C KRB buffer containing 1 μCi/mL [^{3}H]-2-deoxy-D-glucose (PerkinElmer, Cat. No. NET54900), 1 mM 2-deoxy-Dglucose, 0.3 μCi/mL [^{14}C]-mannitol (PerkinElmer, Cat. No. NEC314), and 7 mM mannitol plus or minus insulin (50 mU/mL) for 10 min. Submaximal insulin-stimulated glucose uptake was also measured in EDL muscles using a slightly different protocol that included preincubation in KRB buffer for 60 min, an additional 20 min in the presence or absence of submaximal insulin (600 μU/mL), and, finally,

to assess glucose uptake, 10 min incubation in continuously gassed, 30°C KRB buffer containing 1.5 μCi/mL [^{3}H]-2-deoxy-D-glucose, 1 mM 2-deoxy-D-glucose, 0.45 μCi/mL [^{14}C]-mannitol, and 7 mM mannitol. At the conclusion of all incubations, muscles were frozen in liquid nitrogen, weighed, solubilized in 1 N NaOH at 80°C for 15 min, and finally neutralized with 1 N HCl. The remaining fraction was centrifuged at 10,000 *g* for 1 min. Aliquots were removed for scintillation counting of the [^{3}H] and [^{14}C] labels, and [^{3}H]-2-deoxyglucose uptake was calculated.

Permeabilized Muscle Fiber Bundle Preparation

This technique was performed as previously described (27, 33, 34). Briefly, portions of RG and WG were dissected and immediately placed in ice-cold buffer X (50 mM K-MES, 35 mM KCl, 7.23 mM K_2EGTA, 2.77 mM CaK_2EGTA, 20 mM imidazole, 20 mM taurine, 5.7 mM ATP, 14.3 mM phosphocreatine, and 6.56 mM $MgCl_2$-$6H_2O$, pH 7.1) for separation with needle-tip forceps under a dissecting microscope. Separated fiber bundles were incubated on a rocker in buffer X containing 30 μg/mL saponin for 30 min at 4°C. The fibers were then transferred to buffer Z (105 mM K-MES, 30 mM KCl, 1 mM EGTA, 10 mM K_2HPO_4, 5 mM $MgCl_2$-$6H_2O$, 0.5 mg/mL BSA, pH 7.1) and incubated on the rocker at 4°C for at least 20 min or until experimentation (<45 min). At the conclusion of the experiment, fibers were rinsed in dH_2O, placed in empty tubes with perforated caps, and freeze-dried to determine dry weights.

Mitochondrial Respiration (JO_2), $\Delta\Psi_m$, and JH_2O_2 Measurements

A high-resolution respirometer (O2K, OROBOROS Innsbruck, Austria) equipped with a conditioned tetraphenylphosphonium (TPP)-selective electrode was used to measure $\Delta\Psi_m$ and JO_2 simultaneously as previously described (33). All O2K experiments were performed in buffer Z supplemented with 20 mM creatine monohydrate (to clamp ADP concentrations) and 25 μM blebbistatin [to inhibit contraction (35)]. For $\Delta\Psi_m$-JO_2 experiments, lipid substrates, L-carnitine (5 mM), and 1.1 μM TPP were included in the buffer during the background phase. Once stable, serial additions of TPP (final concentrations 1.15, 1.20, 1.25, and 1.30 μM) were made to generate a standard curve before addition of the PmFB. Mitochondrial JH_2O_2 production was measured fluorometrically (FluoroMax/Fluorolog spectrofluorometers, HORIBA Jobin Yvon) in buffer Z supplemented with 10 μM Amplex UltraRed (Invitrogen), 1 U/mL horseradish peroxidase (Sigma), 20 U/mL CuZn SOD (Sigma), and 25 μM blebbistatin. Both auranofin (500 μM; thioredoxin reductase inhibitor) and carmustine (100 μM; glutathione reductase inhibitor) were added fresh to inhibit the redox buffering system (36). All H_2O_2 data therefore represent JH_2O_2 production.

Measurements of Redox State

Reduced (GSH) and oxidized (GSSG) glutathione concentrations were measured by a standard assay (Oxis International, Inc.) with minor modifications. Mouse TA or EDL muscles were homogenized in TE buffer (10 mM Tris-base, 1 mM EDTA, pH 7) with protease and phosphatase inhibitor cocktails added (Sigma products: P8340, P5726, and P0044). TE buffer was bubbled with $N_{2(g)}$ for 15 min before homogenizing the muscle. Frozen muscles were submerged in TE buffer, minced with scissors, and homogenized with a hand-pestle for 1 min. Then, 200 μL of muscle homogenate was immediately added to a tube containing the alkylating agent 1-methyl-2-vinylpyridinium trifluoromethanesulfonate (M2VP, final concentration 0.5 mM) and vortexed. The M2VP-treated aliquot was used to measure GSSG undiluted, whereas the remaining homogenate was diluted 20× in TE buffer to measure GSH. A 96-well plate was loaded with 25 μL of sample/standard followed by 25 μL each of the kit enzyme and chromagen solutions and incubated at RT for 10 min with gentle shaking. The absorbance at 412 nm was measured immediately after 25 μL of reconstituted NADPH was added to each well every minute for 4 min. Data analysis was conducted according to product guidelines.

Protein Analysis by Western Blot

Reduced, oxidized-dimer, and oxidized-decamer forms of peroxiredoxin-2 (Prx2, cytosolic) and Prx3 (mitochondrial) were measured in TA and EDL homogenates by standard nonreducing Western blot analysis (37). Frozen muscles were homogenized in the same fashion as GSH/GSSG samples except the buffer included 0.5 mM M2VP for TAs or 5 mM *N*-ethylmaleimide (NEM) for EDLs (either alkylating agent is sufficient for these experiments). Ponceau S stain was used to verify equal protein load (50 μg/well) and consistent gel transfer. Anti-Prx2 (AbCam, ab109367) and anti-Prx3 (AbFrontier, LF-MA0044) were used for protein detection as previously described (37). Blots were imaged using a Li-Cor IR imager and quantified using Image Studio Lite (V. 5.0, Li-Cor Bioscience). A representative blot is shown in Supplemental Fig. S5; all Supplemental material is available at https://doi.org/10.6084/m9.figshare.13550465. Relative band intensities are presented (only the top band quantified in apparent doublets). As a positive control, samples were treated with the reducing agent β-mercaptoethanol (20× dilution) to verify oxidized and reduced Prx bands. Oxidized decamer (~250 kD), oxidized dimer (~35–42 kD), and reduced (20–25 kD) forms of Prx2 and Prx3 were quantified and presented as fold difference relative to controls.

Additional immunoblot analyses were performed to assess insulin signaling and glucose regulatory protein levels as previously described (38–40). Plantaris muscles were incubated in KRB buffer for 60 min as described earlier for glucose uptake assays, followed by an additional 20 min in the presence or absence of submaximal insulin (600 μU/mL). Muscles were then frozen and homogenized in buffer containing 20 mM Tris-HCl pH 7.5, 5 mM EDTA, 10 mM $Na_4P_2O_7$, 100 mM NaF, 2 mM $NaVO_4$, 0.0015 mM aprotinin, 0.01 mM leupeptin, 3 mM benzamidine, 1 mM phenylmethylsulfonylfluoride, and 1% IGEPAL CA-630. Samples were rotated end-over-end at 4°C for 60 min and centrifuged at 13,000 *g* for 30 min. Lysate protein concentrations were determined via the Bradford method using Bio-Rad protein assay dye (Cat. No. 5000006, Bio-Rad Laboratories, Hercules, CA). Lysates (20 μg) were loaded for SDS-PAGE, and proteins were transferred onto 0.2-μm nitrocellulose membranes. Ponceau S solution (Cat. No. P7170, Sigma-Aldrich, St. Louis, MO) was utilized to assess equal protein loading and transfer. Anti-

hexokinase II (Santa Cruz, sc-6521), anti-GLUT4 (Millipore, 07–1404), anti-p-AKT (Thr308; Cell Signaling, 9275S), anti-total-AKT (Cell Signaling, 4685S), anti-p-AS160 (TBC1D4; Cell Signaling, 07–741), and anti-total-AS160 (p-TBC1D4-Thr642; Millipore, 8881) were used for protein detection. Densitometric analysis of immunoblots was performed using a Bio-Rad Chemidoc XRS + imaging system and Bio-Rad Image Lab software v. 6.0.1 (Bio-Rad Laboratories, Hercules, CA).

Statistics

Unpaired Student's *t* test assuming equal distributions and ANOVAs (where appropriate) were used for all analyses followed by Tukey's multiple-comparison post hoc tests. Data are presented as means ± SE. Significance was set at $P < 0.05$.

RESULTS

Muscle-Specific Overexpression of PPARα on the B6N Strain

Transgenic mice overexpressing PPARα in muscle on a B6J background are characterized by increased fatty acid oxidation rates, marked glucose intolerance, and muscle insulin resistance, even on a low-fat diet (20). To study the impact of PPARα overexpression in muscle without the potential confounding influence of the numerous genetic differences present in the B6J strain, including the absence of mitochondrial nicotinamide nucleotide transhydrogenase (NNT) (41, 42), muscle-specific MCK-PPARα (B6J) mice were backcrossed to the full congenic B6N strain. Similar to MCK-PPARα (B6J) mice (20), MCK-PPARα (B6N) mice had similar whole body and fat mass but lower lean mass compared with WT (B6N) controls (Supplemental Fig. S1). Respiratory exchange ratio (RER) was lower during the daytime period (light cycle), confirming elevated flux through fatty acid oxidation. Interestingly, energy expenditure was also higher during the light cycle in MCK-PPARα (B6N) versus WT (B6N) mice (Supplemental Fig. S1), whereas food intake (24 h) and physical activity (light or dark cycle) were not different (not shown).

Similar to MCK-PPARα (B6J) mice (20), MCK-PPARα (B6N) mice were also characterized by lower glucose tolerance relative to WT (B6N) controls (Fig. 1*A*). Both basal and maximal insulin-stimulated 2-deoxyglucose uptake rates were lower in the soleus and EDL muscles from MCK-PPARα (B6N) mice (Fig. 1*B*). The net response to insulin however (maximal insulin-stimulated minus basal) was either not different (soleus) or only slightly lower (EDL), suggesting that overexpression of PPARα in the B6N background elicited an overall depression in muscle glucose uptake rather than insulin resistance per se.

Impact of MCK-PPARα Overexpression on Mitochondrial $\Delta\Psi_m$, JO_2, and JH_2O_2

To determine the potential impact of PPARα overexpression on skeletal muscle mitochondrial function, mitochondrial $\Delta\Psi_m$, JO_2, and JH_2O_2 were measured in PmFBs from RG and WG during respiration supported exclusively by 20 μM palmitoyl-CoA, 18 μM palmitoyl-carnitine, and 5 mM carnitine. In preliminary experiments, this substrate combination was found to maximize flux through β-oxidation. During non-ADP-stimulated (state 4) respiration, $\Delta\Psi_m$ and JO_2 were similar in RG PmFBs from MCK-PPARα (B6N) and WT (B6N) controls (Fig. 1*C*). In WG PmFBs from WT (B6N) mice, however, $\Delta\Psi_m$ and JO_2 were markedly lower (filled circle, Fig. 1*D*), suggesting that flux through β-oxidation alone in muscle composed primarily of glycolytic fibers is insufficient, in-and-of-itself, to fully charge the membrane potential and support state 4 respiration. Interestingly, overexpression of PPARα increased both lipid-supported $\Delta\Psi_m$ and JO_2 in WG to values obtained in WT (B6N) controls when respiration was supported by carbohydrate-based substrates (i.e., pyruvate + glutamate + malate, open circle Fig. 1*D*), suggesting that the increase in the capacity for β-oxidation induced by PPARα overexpression in WG fibers provided sufficient reducing equivalents to fully charge the mitochondria. PPARα overexpression also increased maximal fatty acid-supported ADP-stimulated (state 3) JO_2 in both RG and WG PmFBs (Fig. 1*E*), confirming an overall increase in β-oxidative flux capacity in the muscles of MCK-PPARα (B6N) mice.

Mitochondrial respiration rate is governed by demand, which in turn dictates the rate at which electrons are drawn by the electron transport chain from catabolic pathways. Allosteric control mechanisms regulate the relative reliance on specific pathways as well as limit flux when supply exceeds demand to minimize hyper-reduction of the ETS and superoxide/H_2O_2 production (43). Thus, genetically engineering an increase in β-oxidation flux capacity through overexpression of PPARα could disrupt the normal balance between mitochondrial energy supply and demand. To test this hypothesis, mitochondrial JH_2O_2 production was measured under state 4 conditions identical to the $\Delta\Psi_m$ and JO_2 experiments described earlier. JH_2O_2 production was approximately twofold higher in both RG and WG PmFBs (Fig. 1*F*), providing evidence that genetically engineering an increase in flux through β-oxidation, in the absence of any change in energy demand, increases mitochondrial reductive stress and oxidant production.

PPARα Overexpression Increases Oxidation of Redox Markers

The glutathione redox buffering system is thought to be an ideal marker of intracellular redox environment (44). Interestingly, both reduced (GSH) and oxidized (GSSG) glutathione were either increased or tended to be increased in TA and EDL muscles from MCK-PPARα (B6N) relative to WT (B6N) mice (Fig. 2, *A* and *C*), suggesting an increase in oxidant burden as well as a compensatory response to maintain the GSH/GSSG ratio constant (Fig. 2*E*). Another key antioxidant protein and marker of the intracellular redox environment is the peroxiredoxin (Prx) family of peroxidases (37). Prxs have high rate constants, suggesting this class of proteins may serve as the first line of defense against elevated JH_2O_2 production (45). In the reduced form, typical 2-Cys Prxs (Prx1-4) exist as monomers of ~20–30 kD. When oxidized to the sulfenic acid oxidation state by a single molecule of H_2O_2, Prxs form obligate homodimers. Under high H_2O_2 concentrations, typical 2-Cys Prxs are hyperoxidized to

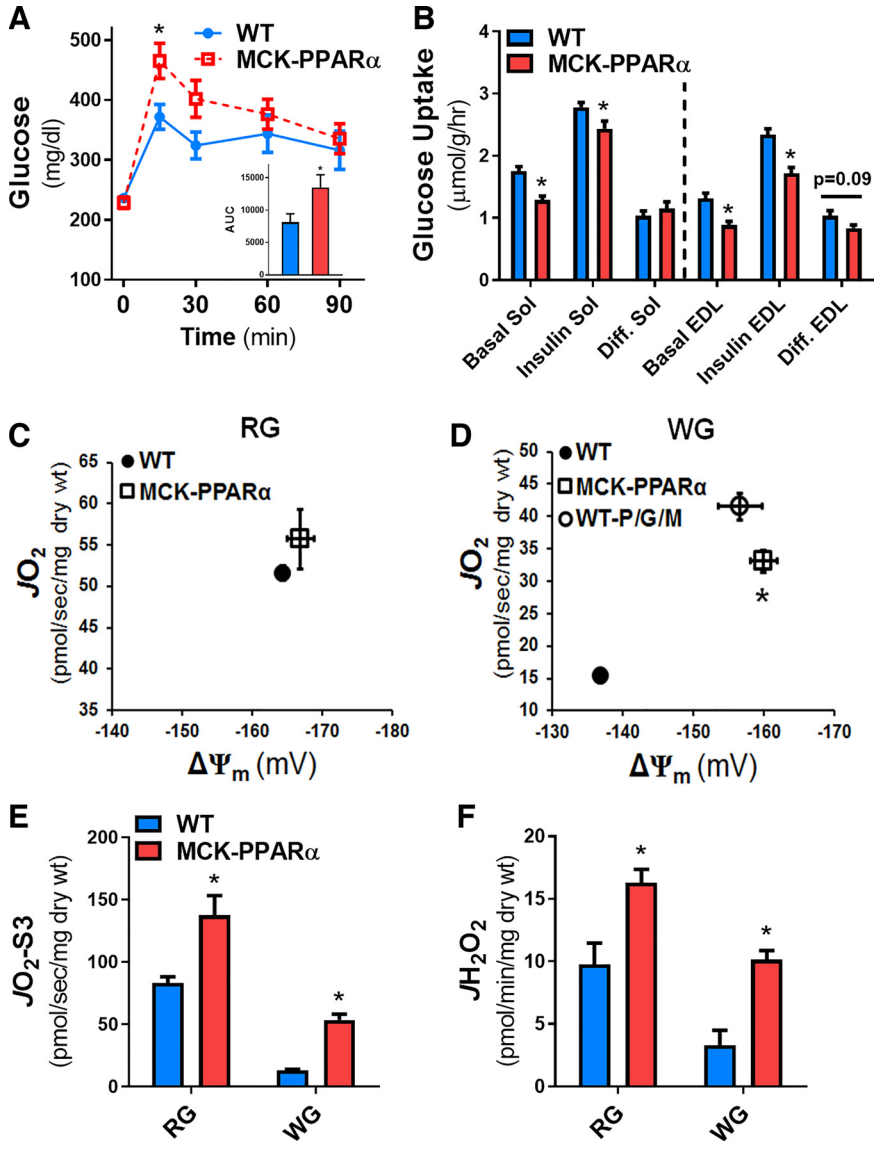

Figure 1. Muscle-specific overexpression of PPARα (MCK-PPARα B6N) increases basal flux through β-oxidation, H_2O_2 emission, and glucose intolerance in chow-fed mice. *A*: blood glucose concentrations following intraperitoneal glucose injection and area under the curve (AUC; *inset*) normalized to baseline values ($n = 9$ or 13 mice/group). *B*: rates of basal and insulin-stimulated ^{3}H-2-deoxyglucose uptake into isolated soleus (Sol) and extensor digitorum longus (EDL) muscles ($n = 7$ or 9 mice/group). The difference (Diff.) between insulin-stimulated and basal rates is also plotted. Values are means ± SE; $^*P < 0.05$ compared with WT. *C* and *D*: JO_2 and $\Delta\Psi_m$ were measured simultaneously under state 4 conditions in permeabilized fiber bundles (PmFBs) prepared from red (RG) and white (WG) portions of the gastrocnemius muscle and supported by 20 μM palmitoyl-CoA, 18 μM palmitoyl-carnitine, and 5 mM carnitine (closed circle: WT; open square: MCK-PPARα). The open circle in *D* represents PmFBs prepared from WT WG supported by 1 mM pyruvate, 10 mM glutamate, and 2 mM malate. *E* and *F*: maximal state 3 (1 mM ADP) JO_2 (*E*) and state 4 JH_2O_2 (*F*) production were measured under identical lipid substrate conditions as in *C* and *D*. Data are means ± SE; $^*P < 0.05$ compared with WT; $n = 5$ or 11 mice/group.

the sulfinic ($-SO_2$) or sulfonic ($-SO_3$) acid oxidation state that prevents dimerization and favors decamer formation detectable by Western blot analysis (37, 46, 47). PPARα overexpression decreased the levels of reduced Prx2 (cytosolic) and Prx3 (mitochondrial), whereas the level of oxidized-dimer Prx2 ($Prx2^{dim}$) increased (Fig. 2, *B* and *E*). There were no differences in $Prx3^{dim}$ or oxidized decamers for either Prx3 or Prx 2 between genotypes. These findings are consistent with the increase in JH_2O_2 production observed in PmFBs in vitro and suggest that PPARα overexpression induced a mild-to-moderate increase in mitochondrial oxidant production in vivo, resulting in a mild-to-moderate shift in the cytosolic redox environment to a more oxidized state.

Lipin-1 Deficiency, Another Model of Increased Flux through Fatty Acid Oxidation

As an additional means of testing whether elevated flux through β-oxidation alters mitochondrial function in skeletal muscle, PmFBs were prepared from lipin-1-deficient mice, a genetic model resulting from a spontaneous mutation in the *Lpin1* gene that is characterized by reduced adiposity, enhanced expression of β-oxidation genes in muscle, increased reliance on fat oxidation, and severe glucose intolerance and insulin resistance (22, 24, 25). Lipid-supported state 4 JO_2 and JH_2O_2 were both higher in RG and WG PmFBs from lipin-1-deficient mice (Fig. 3, *A* and *B*), indicating the potential for elevated basal flux through mitochondrial β-oxidation. Lipin-1 deficiency also increased lipid-supported state 3 respiration in WG PmFBs (Fig. 3*B*), similar to the greater β-oxidation flux capacity observed in PPARα-overexpressing mice. Total muscle GSH and GSSG concentrations were not different between genotypes (data not shown). However, muscle $Prx3^{dim}$ and $Prx3^{deca}$ levels were significantly increased in lipin-1-deficient mice (Fig. 3*C*), indicative of a more oxidized mitochondrial redox state. Interestingly, the reduced form of Prx3 was also elevated, reflecting a potential compensatory response. On the other hand, the reduced form of cytosolic Prx2 was undetectable in both the control ($Lpin1^{+/-}$) and lipin-1-deficient mice, whereas the oxidized form, $Prx2^{dim}$, was elevated in lipin-1-

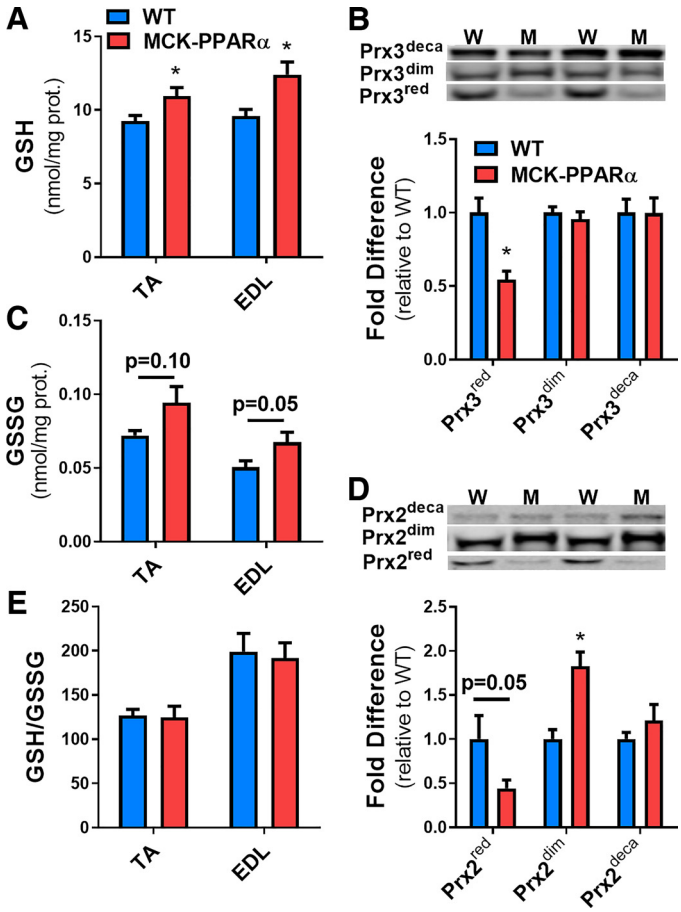

Figure 2. GSH/GSSG and reduced/oxidized Prx2/3 in WT and MCK-PPARα (B6N) muscle homogenates. *A, C,* and *E*: total GSH (*A*) and GSSG (*C*) concentrations were measured in muscle homogenates prepared from frozen TA and EDL muscle. The resulting GSH/GSSG ratios (*E*) are also presented. *B* and *D*: relative levels of reduced (Prx^{red}), oxidized-dimer (Prx^{dim}), and oxidized-decamer (Prx^{deca}) for Prx3 (*B*) and Prx2 (*D*) protein measured in muscle homogenates by nonreducing Western blot analysis. Representative blots are included above each graph (W = WT; M = MCK-PPARα). Data are means ± SE; $^*P < 0.05$ compared with WT; $n = 7$ or 9 mice/group. EDL, extensor digitorum longus; TA, tibialis anterior.

deficient mice (Fig. 3*D*), again consistent with an overall increase in oxidant burden.

Effect of PPARα Overexpression in the Context of High-Fat Diet

To determine if overexpression of PPARα on a B6N background may "hypersensitize" mice to high-fat-diet-induced glucose intolerance, MCK-PPARα-overexpressing mice were studied following 8 wk on a high-fat diet (45% kcal fat, Research Diets, Inc., D12451). Remarkably, total body weight and fat and lean body mass were lower in high fat-fed MCK-PPARα mice (Fig. 4*A*). Food intake measurements proved unreliable in the present study; however, Finck et al. (20) did report similar food intake between MCK-PPARα and WT mice, suggesting that the combination of PPARα overexpression and high-fat diet somehow elevates energy expenditure. Glucose tolerance was slightly better in MCK-PPARα versus WT mice (glucose dose based on lean mass; Fig. 4*B*). Similar to data from low-fat-fed mice (Fig. 1), mitochondrial fatty acid oxidation capacity was enhanced by PPARα overexpression, as evidenced by higher lipid-supported basal $\Delta\Psi_m$ and JO_2 (Fig. 4, *C* and *D*) and higher ADP-stimulated JO_2 (Fig. 4*E*) in both RG and WG muscles, coinciding with higher JH_2O_2 production (Fig. 4*F*) and a mild-to-moderate oxidative shift in redox environment relative to WT mice fed a high-fat diet (Supplemental Fig. S2).

Mitochondria-Targeted Catalase Rescues the MCK-PPARα Phenotype

To determine if the elevated mitochondrial H_2O_2 production in muscle induced by PPARα overexpression (Fig. 1*F*) accounts for the phenotypic differences between the genotypes, MCK-PPARα (B6N) mice were crossed with mice overexpressing catalase, targeted to the mitochondria [MCAT (B6N) (32)] to produce MCK-PPARα/MCAT (B6N) double transgenic (DTG) mice. The presence of MCAT rescued the glucose-intolerant phenotype associated with PPARα overexpression (Fig. 5*A*), which coincided with a normalization of mitochondrial JH_2O_2 production in both permeabilized RG and WG muscles (Fig. 5, *C* and *E*) in the face of persistently elevated fatty acid oxidation rates (i.e., state 4 JO_2 in Fig. 5, *C* and *E*, and elevated $\Delta\Psi_m$ in Supplemental Fig. S3). Although the ratio of GSH/GSSG was not different between genotypes (not shown, similar to Fig. 3*E*), overexpression of catalase did restore $Prx3^{red}$, $Prx3^{dim}$, $Prx2^{red}$, and $Prx3^{dim}$ to control levels (Fig. 5, *D* and *F*), consistent with a normalization of redox homeostasis in the context of PPAR overexpression. Surprisingly, however, both basal and insulin-stimulated glucose uptake rates remained depressed in DTG mice despite the overexpression of catalase (Fig. 5*B*), suggesting that factors other than redox homeostasis contribute to the overall depression in muscle glucose uptake with PPARα overexpression. To further explore the underlying mechanism, we quantified several proteins involved in glucose metabolism and insulin signaling. Muscle GLUT4 protein levels overall were lower in DTG compared with WT and MCK-PPARα (B6N) mice, whereas hexokinase II levels were not different between genotypes (Supplemental Fig. S4). Interestingly, muscle from PPARα-overexpressing mice, regardless of the presence of catalase, were characterized by marked increases in total and insulin-stimulated phospho-AKT (Thr308) and phospho-AS160 (Thr642) levels (Fig. 6, *A–D*). However, the phospho/total ratio for both AKT and AS160 under basal and insulin-stimulated conditions was similar across genotypes. These findings suggest that the PPARα-driven increase in muscle fatty acid oxidation triggers a compensatory increase in the expression of these insulin-signaling proteins in an attempt to restore glucose uptake.

DISCUSSION

The present study reveals that genetically engineering an increase in skeletal muscle β-oxidation capacity increases the relative reliance on fatty acid oxidation at the whole body level in vivo and drives an increase in muscle mitochondrial $\Delta\Psi_m$ and JH_2O_2 emission during fatty acid-supported respiration in vitro. In the context of a normal low-fat diet, this shift in the balance of fuel utilization is associated with an increase in energy expenditure rate, a reduced lean

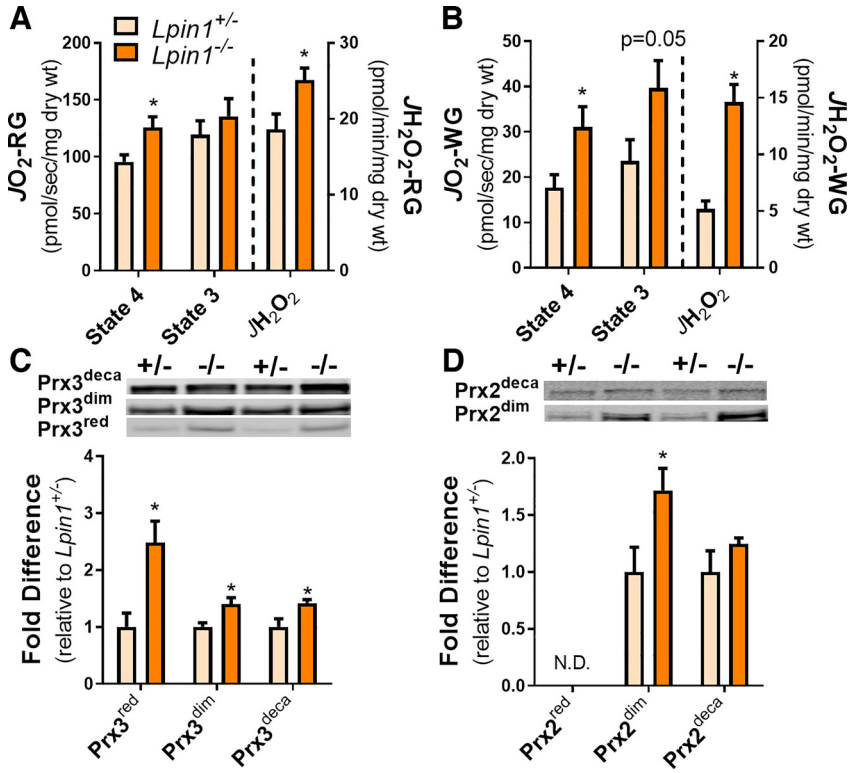

Figure 3. Lipid-supported JO_2 and JH_2O_2 production and Prx2/3 redox states in lipin-1-deficient (*Lpin1*$^{-/-}$) mouse muscle. *A* and *B*: JO_2 (left *y*-axis) and JH_2O_2 (right *y*-axis) were measured in parallel experiments in permeabilized fiber bundles (PmFBs) prepared from red (RG) (*A*) and white (WG) (*B*) portions of the gastrocnemius muscle from *Lpin1*$^{+/-}$ and *Lpin1*$^{-/-}$ mice. PmFBs were supported by 20 μM palmitoyl-CoA, 18 μM palmitoyl-carnitine, 5 mM carnitine, and 1 mM ADP (only for state 3 JO_2). *C* and *D*: relative levels of reduced (Prx^{red}), oxidized-dimer (Prx^{dim}), and oxidized-decamer (Prx^{deca}) for Prx3 (*C*) and Prx2 (*D*) protein measured in muscle homogenates by nonreducing Western blot analysis. Representative blots are included above each graph. Data are means ± SE; $*P < 0.05$ compared with *Lpin1*$^{+/-}$; $n = 7$ or 8 mice/group.

mass, a more oxidized skeletal muscle redox environment, and the development of whole body glucose intolerance that coincides with reduced muscle glucose uptake. Genetically enhancing mitochondrial H_2O_2 scavenging by co-expression of mitochondria-targeted catalase normalizes mitochondrial JH_2O_2 production in vitro and restores both muscle redox environment and whole body glucose tolerance in vivo, consistent with prior studies linking mitochondrial H_2O_2 production and oxidative stress to high-fat-diet-induced insulin resistance (27–31, 48, 49). Surprisingly, however, despite the overexpression of catalase, both basal and absolute insulin-stimulated rates of glucose uptake in muscle remained depressed. Also surprising was that both total and insulin-simulated phospho-AKT and AS160 expression were elevated in muscle of both MCK-PPARα and DTG mice, consistent with at least an attempted compensatory response. Moreover, placing MCK-PPARα mice on a high-fat diet, instead of causing weight gain, elicited significant loss of whole body, fat, and lean mass and a slight improvement in whole body glucose tolerance relative to WT mice. Together the findings provide additional evidence that genetically driving an increase in muscle fatty acid oxidation in the context of a normal low-fat diet increases mitochondrial reductive stress and cellular oxidant burden and decreases muscle glucose uptake and whole body glucose tolerance. However, the persistent decrease in basal and insulin-stimulated glucose uptake in skeletal muscle of MCK-PPARα mice, coupled with the phenotype when fed a high-fat diet, suggests that overexpression of PPARα in muscle imposes a more extensive metabolic stress than experienced by wild-type mice on a high-fat diet.

The mitochondrial dysfunction model of insulin resistance gained prominence more than 15 years ago based on the associative links observed between insulin resistance, cytosolic lipid accumulation, and lower mitochondrial "function" (11), the latter characterized by decreased mitochondrial enzyme activity and fatty acid oxidation capacity measured in muscle homogenates in vitro (4, 50–52) and lower rates of muscle ATP synthesis and substrate oxidation measured by MRS at rest in vivo (6,7, 53). That mitochondrial insufficiency represents an underlying cause of cytosolic bioactive lipid accumulation and insulin resistance, however, has been challenged both conceptually (54–56) and experimentally (57–63). Moreover, mitochondrial respiration is governed by energy demand, not supply, so in theory, merely altering the percent reliance between carbohydrate- and lipid-based substrates without changing the overall rate of reducing equivalent supply (i.e., ΔG_{redox}) should have a minimal effect on the system. For example, disruption of the muscle CDP-ethanolamine pathway (deletion of CTP:phosphoethanolamine cytidylyltransferase gene) disrupts phospholipid synthesis and thereby diverts fatty acids to alternative pathways, inducing intramyocellular and membrane-bound diacylglycerol accumulation and greater reliance on fatty acid oxidation when mice are placed on a high-fat diet (64). However, despite an increase in muscle mitochondrial content and oxidative capacity, energy expenditure and insulin sensitivity are normal in standard chow-fed mice, and insulin resistance in response to high-fat feeding develops similarly in the wild-type and knockout mice (64). In MCK-PPARα mice on a low-fat diet [present study and Ref. (20)], the increase in expression of mitochondrial β-oxidation enzymes appears to drive a

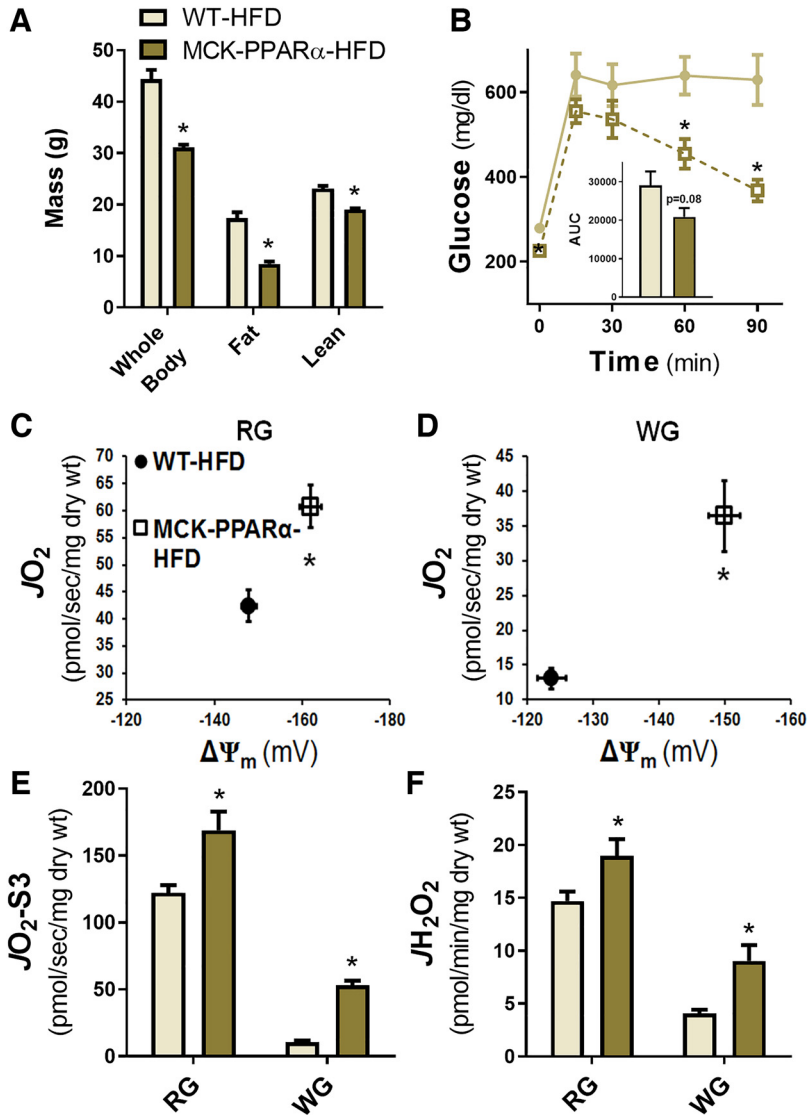

Figure 4. High-fat diet (HFD) induces marked metabolic stress in MCK-PPARα (B6N) mice. *A*: whole body, fat, and lean mass of WT and MCK-PPARα mice treated for 8 wk with HFD. *B*: blood glucose concentrations following intraperitoneal glucose injection (2.5 g/kg fat-free mass) and area under the curve (AUC) normalized to baseline values. *C* and *D*: JO_2 and $\Delta\Psi_m$ measured simultaneously under state 4 conditions in permeabilized fiber bundles from red (RG) (*C*) and white (WG) (*D*) portions of the gastrocnemius muscle and supported by 20 μM palmitoyl-CoA, 18 μM palmitoyl-carnitine, and 5 mM carnitine. *E* and *F*: in separate PmFBs, state 3 (1 mM ADP) JO_2 (*E*) and state 4 JH_2O_2 (*F*) were measured under identical substrate conditions as *C* and *D*. Data are means ± SE; $^*P < 0.05$ compared with WT; $n = 8$ mice/group.

higher absolute (i.e., higher VO_2 and energy expenditure) and relative (i.e., lower RER) flux through β-oxidation in excess of demand (i.e., no change in activity level), resulting in increased supply-side reductive stress/pressure (i.e., ΔG_{redox}), elevated H_2O_2 generation, and more oxidized redox environment, which may at least partially contribute to the decrease in glucose tolerance and muscle glucose uptake. Similar effects have been observed in WT rodents exposed to high-fat diets or high lipid loads (27, 60, 65), suggesting that high-fat diets may affect muscle glucose uptake through a similar mechanism. Conversely, blocking fatty acid entry into muscle mitochondria limits flux through β-oxidation, increases intramyocellular accumulation of bioactive lipids, but preserves or enhances insulin sensitivity even in the context of a high-fat diet (20, 63, 66).

The bioenergetics of fat oxidation underscores the susceptibility of mitochondrial and cytosolic redox environments to oxidative stress when flux through β-oxidation is accelerated. Fatty acids are the most electron dense of all the metabolic substrates oxidized by muscle, placing greater reducing pressure on the ETS per mole of substrate. Being matrix contained, the reducing equivalents generated by fatty acid oxidation are almost entirely obligated to be oxidized by the ETS, thus increasing reductive stress and the potential for electron leak within the system. Glucose, on the other hand, is less electron dense, and oxidation takes place in both cytosolic and matrix compartments. The advantage of the cytosolic compartment in minimizing oxidant production is the presence of the pentose phosphate pathway enzymes and lactate dehydrogenase, both of which minimize reducing pressure on the ETS by shunting glucose and NADH oxidation to anabolic and anaerobic pathways during periods of low energetic demand. Besides the ETS, increased flux through β-oxidation poses additional risk for electron leak upstream because the acyl-CoA dehydrogenase-linked $FADH_2$ is not only intrinsically more prone to single electron loss, but both MCAD and VLCAD have been shown to generate oxidants during electron transfer to the electron transfer flavoprotein independent of $\Delta\Psi_m$ or other components of the ETS (67, 68).

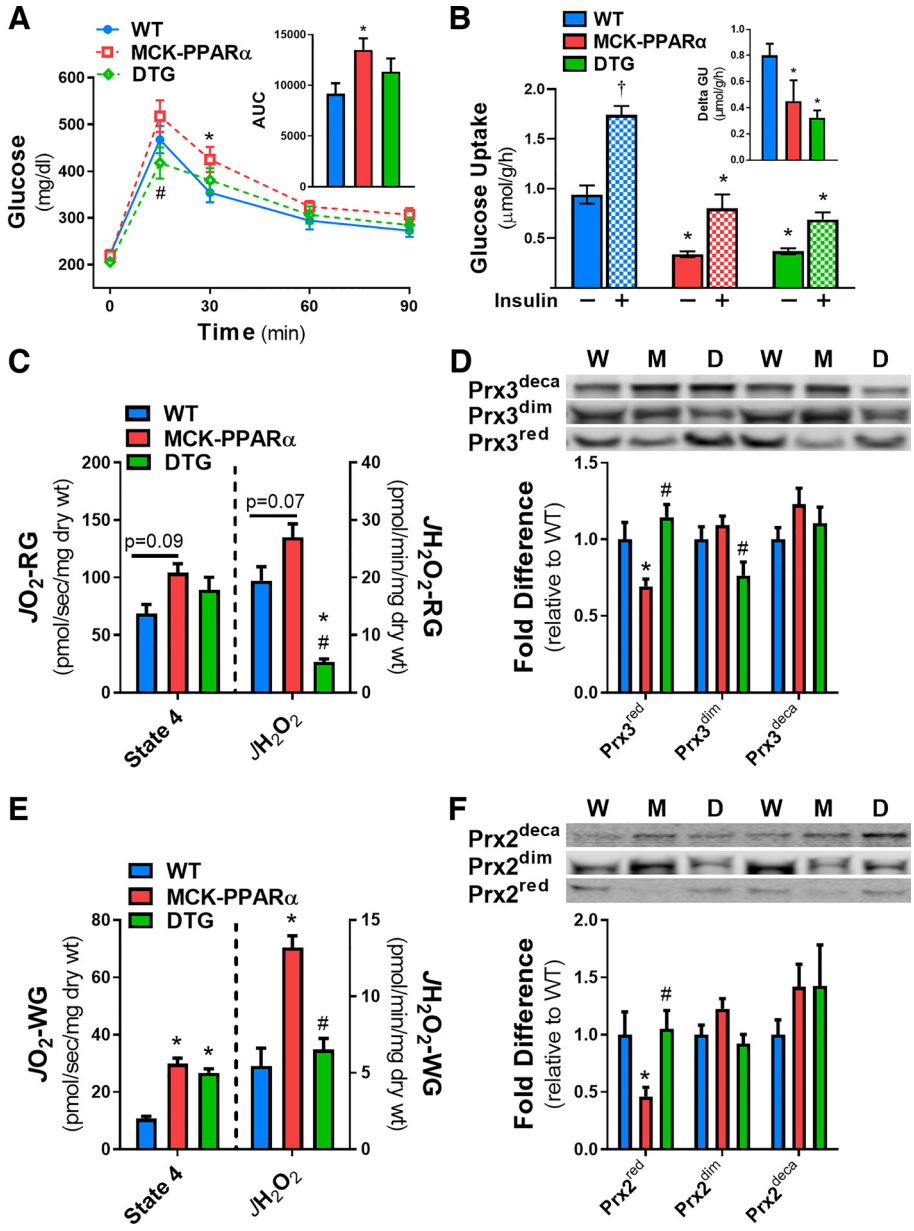

Figure 5. Glucose tolerance, lipid-supported JO_2 and JH_2O_2 production, and Prx2/3 redox states in WT, MCK-PPARα, and MCK-PPARα-MCAT double transgenic (DTG) (B6N) mice. *A*: blood glucose concentrations following intraperitoneal glucose injection and area under the curve (AUC, *inset*) normalized to baseline values ($n = 17$ or 19 mice/group). *B*: rates of basal, insulin-stimulated, and delta (insulin minus basal, *inset*) ^{3}H-2-deoxyglucose uptake into extensor digitorum longus (EDL) muscles ($n = 7$ mice/group). *C* and *E*: state 4 JO_2 (left *y*-axis) and JH_2O_2 (right *y*-axis) measured in parallel experiments during respiration supported by 20 μM palmitoyl-CoA, 18 μM palmitoyl-carnitine, and 5 mM carnitine in permeabilized fiber bundles from red (RG) (*C*) and white (WG) (*E*) portions of the gastrocnemius muscle ($n = 6$ or 7 mice/group). *D* and *F*: relative levels of reduced (Prx^{red}), oxidized-dimer (Prx^{dim}), and oxidized-decamer (Prx^{deca}) for Prx3 (*D*) and Prx2 (*F*) protein measured in muscle homogenates by nonreducing Western blot analysis. Representative blots are included (W = WT; M = MCK-PPARα; D = DTG, $n = 6$ or 7 mice/group). Data are means ± SE; $*P < 0.05$ compared with WT; $\#P < 0.05$ compared with MCK-PPARα.

The mechanism by which a more oxidized redox environment interferes with insulin signaling remains elusive; however, the work presented here suggests that the Prx family of antioxidant proteins may play a role in the process. Peroxiredoxins have extraordinarily high rate constants, making them excellent scavengers of H_2O_2 (69). Prxs also associate allosterically with protein kinases and phosphatases, interactions that can change depending on their redox and oligomerization state to affect signaling (45). Alternatively, Prxs may affect insulin signal transduction by forming reversible mixed disulfide bonds with cysteine residues of regulatory or other signal-transducing proteins (45). H_2O_2-induced interdisulfide exchange reactions between Prx cysteines and cysteine thiols of transcription factors have also been suggested as a mechanism for rapidly regulating transcription factor activity (69), which is interesting to consider given the marked upregulation in Akt and AS160 expression. Finally, during high oxidative stress, hyperoxidized Prx decamers have also been reported to undergo a functional shift from peroxidase to protein chaperone as a protective measure against H_2O_2-induced cell death (46, 70). More research is needed to investigate the roles of Prxs as signal transducers or modulators of intracellular signaling, especially since different isoforms, redox states, oligomerization, posttranslational modifications, and cellular compartmentalization may further influence regulation.

A curious finding in the present study was the greater rate of energy expenditure in MCK-PPARα mice, which appeared to be accentuated in the context of a high-fat diet. Similar to a previous report (20), weight gain, lean mass, and fat mass were all markedly lower in MCK-PPARα relative to WT mice

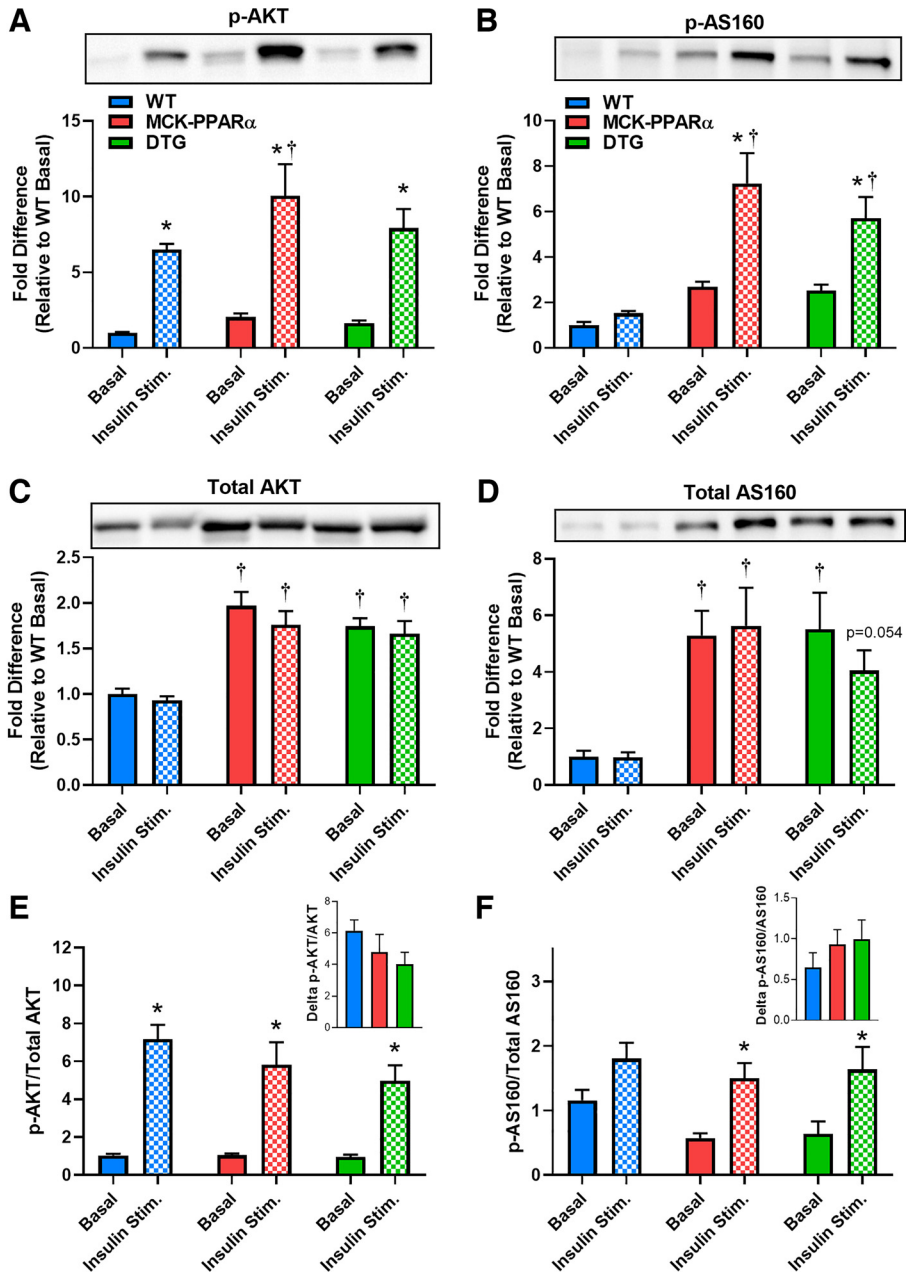

Figure 6. Basal and insulin-stimulated phospho- and total AKT and AS160 in muscle from WT, MCK-PPARα, and MCK-PPARα/MCAT (DTG) mice. *A–F*: relative levels of phospho- (*A*), total (*C*), and the phospho/total ratio (*E*) of AKT and AS160 (*B, D,* and *F*) in basal and insulin-stimulated muscle homogenates measured by Western blot analysis. Representative blots are included (W = WT; M = MCK-PPARα; D = DTG, $n = 6$ or 7 mice/group). Data are means ± SE; $^{*}P < 0.05$ compared with corresponding basal state. $^{\dagger}P < 0.05$ compared with corresponding WT.

on a high-fat diet, implying that driving an increase in flux through β-oxidation in skeletal muscle somehow accelerates energy expenditure, possibly via some type of lipid-induced uncoupling or futile cycling mechanism. Another possibility is that the increase in mitochondrial H_2O_2 production increases flux through redox buffering circuits, which ultimately draws electrons from NADPH to reduce H_2O_2 to $2H_2O$. The resulting $NADP^+$ in turn activates NNT, an inner mitochondrial transmembrane protein that catalyzes the resynthesis of NADPH by drawing on $\Delta\Psi_m$ and thereby expending energy (71). Because the ETS as well as other enzyme complexes (e.g., pyruvate dehydrogenase, succinate dehydrogenase, enzymes in β-oxidation) appear to be ideally suited for sensing energy balance through redox chemistry (26, 72), the ensuing H_2O_2 production and flux through NNT-linked redox buffering circuits represents a potential source of energy expenditure to counterbalance the reductive stress created during nutritional overload (36, 71). Regardless of the mechanism(s), the findings suggest that strategies to prevent or otherwise mitigate reductive stress may be an effective means of preventing or treating metabolic disease stemming from chronic energy surplus.

ACKNOWLEDGMENTS

We thank Dr. Daniel P. Kelly for providing the MCK-PPARα mice.

GRANTS

This work was supported by funding from Einstein-Mt. Sinai National Institutes of Health (NIH) P60 DK020541 (to I. J. K.), NIH F31 DK119080 (to S. L. M.), and NIH R01s DK103562 (to C. A. W.) and DK096907 and DK110656 (to P. D. N).

DISCLOSURES

No conflicts of interest, financial or otherwise, are declared by the authors.

AUTHOR CONTRIBUTIONS

C.D.S., C-T.L., I.J.K., C.A.W., and P.D.N. conceived and designed research; C.D.S., C-T.L., S.L.M., L.A.W., C.A. Schmidt, C.A. Smith, I.J.K., and C.A.W. performed experiments; C.D.S., C-T.L., S.L.M., L.A.W., C.A. Schmidt, C.A. Smith, I.J.K., C.A.W., and P.D.N. analyzed data; C.D.S., C-T.L., S.L.M., C.A.S., I.J.K., C.A.W., and P.D.N. interpreted results of experiments; C.D.S., C.A.S., and P.D.N. prepared figures; C.D.S. and P.D.N. drafted manuscript; C.D.S., C-T.L., C.A.W., and P.D.N. edited and revised manuscript; C.D.S., C-T.L., S.L.M., L.A.W., C. A. Schmidt, C. A. Smith, I.J.K., C.A.W., and P.D.N. approved final version of manuscript.

REFERENCES

1. **Goodpaster BH**, **Kelley DE**, **Thaete FL**, **He J**, **Ross R.** Skeletal muscle attenuation determined by computed tomography is associated with skeletal muscle lipid content. *J Appl Physiol (1985)* 89: 104–110, 2000. doi:10.1152/jappl.2000.89.1.104.
2. **Perseghin G**, **Scifo P**, **De Cobelli F**, **Pagliato E**, **Battezzati A**, **Arcelloni C**, **Vanzulli A**, **Testolin G**, **Pozza G**, **Del MA**, **Luzi L.** Intramyocellular triglyceride content is a determinant of in vivo insulin resistance in humans: a 1H-13C nuclear magnetic resonance spectroscopy assessment in offspring of type 2 diabetic parents. *Diabetes* 48: 1600–1606, 1999. doi:10.2337/diabetes.48.8.1600.
3. **Turner N**, **Kowalski GM**, **Leslie SJ**, **Risis S**, **Yang C**, **Lee-Young RS**, **Babb JR**, **Meikle PJ**, **Lancaster GI**, **Henstridge DC**, **White PJ**, **Kraegen EW**, **Marette A**, **Cooney GJ**, **Febbraio MA**, **Bruce CR.** Distinct patterns of tissue-specific lipid accumulation during the induction of insulin resistance in mice by high-fat feeding. *Diabetologia* 56: 1638–1648, 2013. doi:10.1007/s00125-013-2913-1.
4. **Kelley DE**, **Goodpaster B**, **Wing RR**, **Simoneau JA.** Skeletal muscle fatty acid metabolism in association with insulin resistance, obesity, and weight loss. *Am J Physiol Endocrinol Metab* 277: E1130–E1141, 1999. doi:10.1152/ajpendo.1999.277.6.E1130.
5. **Hulver MW**, **Berggren JR**, **Cortright RN**, **Dudek RW**, **Thompson RP**, **Pories WJ**, **MacDonald KG**, **Cline GW**, **Shulman GI**, **Dohm GL**, **Houmard JA.** Skeletal muscle lipid metabolism with obesity. *Am J Physiol Endocrinol Metab* 284: E741–E747, 2003. doi:10.1152/ajpendo.00514.2002.
6. **Petersen KF**, **Befroy D**, **Dufour S**, **Dziura J**, **Ariyan C**, **Rothman DL**, **DiPietro L**, **Cline GW**, **Shulman GI.** Mitochondrial dysfunction in the elderly: possible role in insulin resistance. *Science* 300: 1140–1142, 2003. doi:10.1126/science.1082889.
7. **Petersen KF**, **Dufour S**, **Befroy D**, **Garcia R**, **Shulman GI.** Impaired mitochondrial activity in the insulin-resistant offspring of patients with type 2 diabetes. *N Engl J Med* 350: 664–671, 2004. doi:10.1056/NEJMoa031314.
8. **Schrauwen-Hinderling VB**, **Kooi ME**, **Hesselink MKC**, **Jeneson JAL**, **Backes WH**, **van Echteld CJA**, **van Engelshoven JMA**, **Mensink M**, **Schrauwen P.** Impaired in vivo mitochondrial function but similar intramyocellular lipid content in patients with type 2 diabetes mellitus and BMI-matched control subjects. *Diabetologia* 50: 113–120, 2007. doi:10.1007/s00125-006-0475-1.
9. **Szendroedi J**, **Schmid AI**, **Chmelik M**, **Toth C**, **Brehm A**, **Krssak M**, **Nowotny P**, **Wolzt M**, **Waldhausl W**, **Roden M.** Muscle mitochondrial ATP synthesis and glucose transport/phosphorylation in type 2 diabetes. *PLoS Med* 4: e154, 2007. doi:10.1371/journal.pmed.0040154.
10. **Holland WL**, **Summers SA.** Sphingolipids, insulin resistance, and metabolic disease: new insights from in vivo manipulation of sphingolipid metabolism. *Endocr Rev* 29: 381–402, 2008. doi:10.1210/er.2007-0025.
11. **Lowell BB**, **Shulman GI.** Mitochondrial dysfunction and type 2 diabetes. *Science* 307: 384–387, 2005. doi:10.1126/science.1104343.
12. **Abu-Elheiga L**, **Matzuk MM**, **Abo-Hashema KA**, **Wakil SJ.** Continuous fatty acid oxidation and reduced fat storage in mice lacking acetyl-CoA carboxylase 2. *Science* 291: 2613–2616, 2001. doi:10.1126/science.1056843.
13. **Abu-Elheiga L**, **Oh W**, **Kordari P**, **Wakil SJ.** Acetyl-CoA carboxylase 2 mutant mice are protected against obesity and diabetes induced by high-fat/high-carbohydrate diets. *Proc Natl Acad Sci USA* 100: 10207–10212, 2003. doi:10.1073/pnas.1733877100.
14. **Choi CS**, **Savage DB**, **Abu-Elheiga L**, **Liu Z-X**, **Kim S**, **Kulkarni A**, **Distefano A**, **Hwang Y-J**, **Reznick RM**, **Codella R**, **Zhang D**, **Cline GW**, **Wakil SJ**, **Shulman GI.** Continuous fat oxidation in acetyl-CoA carboxylase 2 knockout mice increases total energy expenditure, reduces fat mass, and improves insulin sensitivity. *Proc Natl Acad Sci USA* 104: 16480–16485, 2007. doi:10.1073/pnas.0706794104.
15. **Hoehn KL**, **Turner N**, **Swarbrick MM**, **Wilks D**, **Preston E**, **Phua Y**, **Joshi H**, **Furler SM**, **Larance M**, **Hegarty BD**, **Leslie SJ**, **Pickford R**, **Hoy AJ**, **Kraegen EW**, **James DE**, **Cooney GJ.** Acute or chronic upregulation of mitochondrial fatty acid oxidation has no net effect on whole-body energy expenditure or adiposity. *Cell Metab* 11: 70–76, 2010. doi:10.1016/j.cmet.2009.11.008.
16. **Olson DP**, **Pulinilkunnil T**, **Cline GW**, **Shulman GI**, **Lowell BB.** Gene knockout of Acc2 has little effect on body weight, fat mass, or food intake. *Proc Natl Acad Sci USA* 107: 7598–7603, 2010. doi:10.1073/pnas.0913492107.
17. **Chen HC**, **Farese RV Jr.** Turning WAT into BAT gets rid of fat**.** *Nat Med* 7: 1102–1103, 2001. doi:10.1038/nm1001-1102.
18. **Gilliam LAA**, **Neufer PD.** Transgenic mouse models resistant to diet-induced metabolic disease: is energy balance the key? *J Pharmacol Exp Ther* 342: 631–636, 2012. doi:10.1124/jpet.112.192146.
19. **Reitman ML.** Metabolic lessons from genetically lean mice. *Annu Rev Nutr* 22: 459–482, 2002. doi:10.1146/annurev.nutr.22.010402.102849.
20. **Finck BN**, **Bernal-Mizrachi C**, **Han DH**, **Coleman T**, **Sambandam N**, **LaRiviere LL**, **Holloszy JO**, **Semenkovich CF**, **Kelly DP.** A potential link between muscle peroxisome proliferator-activated receptor-alpha signaling and obesity-related diabetes. *Cell Metab* 1: 133–144, 2005. doi:10.1016/j.cmet.2005.01.006.
21. **Peterfy M**, **Phan J**, **Xu P**, **Reue K.** Lipodystrophy in the fld mouse results from mutation of a new gene encoding a nuclear protein, lipin. *Nat Genet* 27: 121–124, 2001. doi:10.1038/83685.
22. **Reue K**, **Xu P**, **Wang XP**, **Slavin BG.** Adipose tissue deficiency, glucose intolerance, and increased atherosclerosis result from mutation in the mouse fatty liver dystrophy (fld) gene. *J Lipid Res* 41: 1067–1076, 2000.
23. **Xu J**, **Lee WNP**, **Phan J**, **Saad MF**, **Reue K**, **Kurland IJ.** Lipin deficiency impairs diurnal metabolic fuel switching. *Diabetes* 55: 3429–3438, 2006. doi:10.2337/db06-0260.
24. **Csaki LS**, **Dwyer JR**, **Li X**, **Nguyen MH**, **Dewald J**, **Brindley DN**, **Lusis AJ**, **Yoshinaga Y**, **de Jong P**, **Fong L**, **Young SG**, **Reue K.** Lipin-1 and lipin-3 together determine adiposity in vivo. *Mol Metab* 3: 145–154, 2014. doi:10.1016/j.molmet.2013.11.008.
25. **Phan J**, **Reue K.** Lipin, a lipodystrophy and obesity gene. *Cell Metab* 1: 73–83, 2005. doi:10.1016/j.cmet.2004.12.002.
26. **Murphy MP.** How mitochondria produce reactive oxygen species. *Biochem J* 417: 1–13, 2009. doi:10.1042/BJ20081386.
27. **Anderson EJ**, **Lustig ME**, **Boyle KE**, **Woodlief TL**, **Kane DA**, **Lin C-T**, **Price JW 3rd**, **Kang L**, **Rabinovitch PS**, **Szeto HH**, **Houmard JA**, **Cortright RN**, **Wasserman DH**, **Neufer PD.** Mitochondrial H_2O_2 emission and cellular redox state link excess fat intake to insulin resistance in both rodents and humans. *J Clin Invest* 119: 573–581, 2009. doi:10.1172/JCI37048.
28. **Fazakerley DJ**, **Chaudhuri R**, **Yang P**, **Maghzal GJ**, **Thomas KC**, **Krycer JR**, **Humphrey SJ**, **Parker BL**, **Fisher-Wellman KH**, **Meoli CC**, **Hoffman NJ**, **Diskin C**, **Burchfield JG**, **Cowley MJ**, **Kaplan W**, **Modrusan Z**, **Kolumam G**, **Yang JY**, **Chen DL**, **Samocha-Bonet D**, **Greenfield JR**, **Hoehn KL**, **Stocker R**, **James DE.** Mitochondrial CoQ deficiency is a common driver of mitochondrial oxidants and insulin resistance. *eLife* 7: e32111, 2018. doi:10.7554/eLife.32111.
29. **Fazakerley DJ**, **Minard AY**, **Krycer JR**, **Thomas KC**, **Stöckli J**, **Harney DJ**, **Burchfield JG**, **Maghzal GJ**, **Caldwell ST**, **Hartley RC**, **Stocker R**, **Murphy MP**, **James DE.** Mitochondrial oxidative stress causes insulin resistance without disrupting oxidative phosphorylation. *J Biol Chem* 293: 7315–7328, 2018. doi:10.1074/jbc.RA117.001254.
30. **Hoehn KL**, **Salmon AB**, **Hohnen-Behrens C**, **Turner N**, **Hoy AJ**, **Maghzal GJ**, **Stocker R**, **Van Remmen H**, **Kraegen EW**, **Cooney GJ**, **Richardson AR**, **James DE.** Insulin resistance is a cellular antioxidant

defense mechanism. *Proc Natl Acad Sci USA* 106: 17787–17792, 2009. doi:10.1073/pnas.0902380106.

31. **Houstis N**, **Rosen ED**, **Lander ES.** Reactive oxygen species have a causal role in multiple forms of insulin resistance. *Nature* 440: 944–948, 2006. doi:10.1038/nature04634.
32. **Schriner SE**, **Linford NJ**, **Martin GM**, **Treuting P**, **Ogburn CE**, **Emond M**, **Coskun PE**, **Ladiges W**, **Wolf N**, **Van Remmen H**, **Wallace DC**, **Rabinovitch PS.** Extension of murine life span by overexpression of catalase targeted to mitochondria. *Science* 308: 1909–1911, 2005. doi:10.1126/science.1106653.
33. **Gilliam LAA**, **Fisher-Wellman KH**, **Lin C-T**, **Maples JM**, **Cathey BL**, **Neufer PD.** The anticancer agent doxorubicin disrupts mitochondrial energy metabolism and redox balance in skeletal muscle. *Free Radic Biol Med* 65: 988–996, 2013. doi:10.1016/j.freeradbiomed.2013.08.191.
34. **Ryan TE**, **Brophy P**, **Lin C-T**, **Hickner RC**, **Neufer PD.** Assessment of in vivo skeletal muscle mitochondrial respiratory capacity in humans by near-infrared spectroscopy: a comparison with in situ measurements. *J Physiol* 592: 3231–3241, 2014. doi:10.1113/jphysiol.2014.274456.
35. **Perry CGR**, **Kane DA**, **Lin C-T**, **Kozy R**, **Cathey BL**, **Lark DS**, **Kane CL**, **Brophy PM**, **Gavin TP**, **Anderson EJ**, **Neufer PD.** Inhibiting myosin-ATPase reveals a dynamic range of mitochondrial respiratory control in skeletal muscle. *Biochem J* 437: 215–222, 2011. doi:10.1042/BJ20110366.
36. **Fisher-Wellman KH**, **Lin C-T**, **Ryan TE**, **Reese LR**, **Gilliam LAA**, **Cathey BL**, **Lark DS**, **Smith CD**, **Muoio DM**, **Neufer PD.** Pyruvate dehydrogenase complex and nicotinamide nucleotide transhydrogenase constitute an energy-consuming redox circuit. *Biochem J* 467: 271–280, 2015. doi:10.1042/BJ20141447.
37. **Cox AG**, **Winterbourn CC**, **Hampton MB.** Measuring the redox state of cellular peroxiredoxins by immunoblotting. *Methods Enzymol* 474: 51–66, 2010. doi:10.1016/S0076-6879(10)74004-0.
38. **Ferey JLA**, **Brault JJ**, **Smith CAS**, **Witczak CA.** Constitutive activation of CaMKKα signaling is sufficient but not necessary for mTORC1 activation and growth in mouse skeletal muscle. *Am J Physiol Endocrinol Metab* 307: E686–E694, 2014. doi:10.1152/ajpendo.00322.2014.
39. **Hinkley JM**, **Ferey JL**, **Brault JJ**, **Smith CAS**, **Gilliam LAA**, **Witczak CA.** Constitutively active CaMKKα stimulates skeletal muscle glucose uptake in insulin-resistant mice in vivo. *Diabetes* 63: 142–151, 2014. doi:10.2337/db13-0452.
40. **McMillin SL**, **Schmidt DL**, **Kahn BB**, **Witczak CA.** GLUT4 is not necessary for overload-induced glucose uptake or hypertrophic growth in mouse skeletal muscle. *Diabetes* 66: 1491–1500, 2017. doi:10.2337/db16-1075.
41. **Fisher-Wellman KH**, **Ryan TE**, **Smith CD**, **Gilliam LAA**, **Lin CT**, **Reese LR**, **Torres MJ**, **Neufer PD.** A direct comparison of metabolic responses to high fat diet in C57BL/6J and C57BL/6NJ mice. *Diabetes* 65: 3249–3261, 2016. doi:10.2337/db16-0291.
42. **Fontaine DA**, **Davis DB.** Attention to background strain is essential for metabolic research: C57BL/6 and the International Knockout Mouse Consortium. *Diabetes* 65: 25–33, 2016. doi:10.2337/db15-0982.
43. **Fisher-Wellman KH**, **Neufer PD.** Linking mitochondrial bioenergetics to insulin resistance via redox biology. *Trends Endocrinol Metab* 23: 142–153, 2012. doi:10.1016/j.tem.2011.12.008.
44. **Schafer FQ**, **Buettner GR.** Redox environment of the cell as viewed through the redox state of the glutathione disulfide/glutathione couple. *Free Radic Biol Med* 30: 1191–1212, 2001. doi:10.1016/s0891-5849(01)00480-4.
45. **Randall LM**, **Ferrer-Sueta G**, **Denicola A.** Peroxiredoxins as preferential targets in H_2O_2-induced signaling. *Methods Enzymol* 527: 41–63, 2013. doi:10.1016/B978-0-12-405882-8.00003-9.
46. **Moon JC**, **Hah Y-S**, **Kim WY**, **Jung BG**, **Jang HH**, **Lee JR**, **Kim SY**, **Lee YM**, **Jeon MG**, **Kim CW**, **Cho MJ**, **Lee SY.** Oxidative stress-dependent structural and functional switching of a human 2-Cys peroxiredoxin isotype II that enhances HeLa cell resistance to H_2O_2-induced cell death. *J Biol Chem* 280: 28775–28784, 2005. doi:10.1074/jbc.M505362200.
47. **Wood ZA**, **Schroder E**, **Harris JR**, **Poole LB.** Structure, mechanism and regulation of peroxiredoxins. *Trends Biochem Sci* 28: 32–40, 2003. doi:10.1016/S0968-0004(02)00003-8.
48. **Lee H-Y**, **Choi CS**, **Birkenfeld AL**, **Alves TC**, **Jornayvaz FR**, **Jurczak MJ**, **Zhang D**, **Woo DK**, **Shadel GS**, **Ladiges W**, **Rabinovitch PS**, **Santos JH**, **Petersen KF**, **Samuel VT**, **Shulman GI.** Targeted expression of catalase to mitochondria prevents age-associated reductions in mitochondrial function and insulin resistance. *Cell Metab* 12: 668–674, 2010. doi:10.1016/j.cmet.2010.11.004.
49. **Paglialunga S**, **Ludzki A**, **Root-McCaig J**, **Holloway GP.** In adipose tissue, increased mitochondrial emission of reactive oxygen species is important for short-term high-fat diet-induced insulin resistance in mice. *Diabetologia* 58: 1071–1080, 2015. doi:10.1007/s00125-015-3531-x.
50. **Kelley DE**, **He J**, **Menshikova EV**, **Ritov VB.** Dysfunction of mitochondria in human skeletal muscle in type 2 diabetes. *Diabetes* 51: 2944–2950, 2002. doi:10.2337/diabetes.51.10.2944.
51. **Kim JY**, **Hickner RC**, **Cortright RL**, **Dohm GL**, **Houmard JA.** Lipid oxidation is reduced in obese human skeletal muscle. *Am J Physiol Endocrinol Metab* 279: E1039–E1044, 2000. doi:10.1152/ajpendo.2000.279.5.E1039.
52. **Patti ME**, **Butte AJ**, **Crunkhorn S**, **Cusi K**, **Berria R**, **Kashyap S**, **Miyazaki Y**, **Kohane I**, **Costello M**, **Saccone R**, **Landaker EJ**, **Goldfine AB**, **Mun E**, **DeFronzo R**, **Finlayson J**, **Kahn CR**, **Mandarino LJ.** Coordinated reduction of genes of oxidative metabolism in humans with insulin resistance and diabetes: potential role of PGC1 and NRF1. *Proc Natl Acad Sci USA* 100: 8466–8471, 2003. doi:10.1073/pnas.1032913100.
53. **Petersen KF**, **Dufour S**, **Shulman GI.** Decreased insulin-stimulated ATP synthesis and phosphate transport in muscle of insulin-resistant offspring of type 2 diabetic parents. *PLoS Med* 2: e233, 2005. doi:10.1371/journal.pmed.0020233.
54. **Holloszy JO.** Skeletal muscle "mitochondrial deficiency" does not mediate insulin resistance. *Am J Clin Nutr* 89: 463S–466S, 2009. doi:10.3945/ajcn.2008.26717C.
55. **Muoio DM**, **Neufer PD.** Lipid-induced mitochondrial stress and insulin action in muscle. *Cell Metab* 15: 595–605, 2012. doi:10.1016/j.cmet.2012.04.010.
56. **Neufer PD.** Cutting fuel offers new clues in diabetic mystery. *J Biol Chem* 294: 12328–12329, 2019. doi:10.1074/jbc.H119.010075.
57. **Ara I**, **Larsen S**, **Stallknecht B**, **Guerra B**, **Morales-Alamo D**, **Andersen JL**, **Ponce-Gonzalez JG**, **Guadalupe-Grau A**, **Galbo H**, **Calbet JAL**, **Helge JW.** Normal mitochondrial function and increased fat oxidation capacity in leg and arm muscles in obese humans. *Int J Obes (Lond)* 35: 99–108, 2011. doi:10.1038/ijo.2010.123.
58. **Fisher-Wellman KH**, **Weber TM**, **Cathey BL**, **Brophy PM**, **Gilliam LAA**, **Kane CL**, **Maples JM**, **Gavin TP**, **Houmard JA**, **Neufer PD.** Mitochondrial respiratory capacity and content are normal in young insulin-resistant obese humans. *Diabetes* 63: 132–141, 2014. doi:10.2337/db13-0940.
59. **Ghosh S**, **Wicks SE**, **Vandanmagsar B**, **Mendoza TM**, **Bayless DS**, **Salbaum JM**, **Dearth SP**, **Campagna SR**, **Mynatt RL**, **Noland RC.** Extensive metabolic remodeling after limiting mitochondrial lipid burden is consistent with an improved metabolic health profile. *J Biol Chem* 294: 12313–12327, 2019. doi:10.1074/jbc.RA118.006074.
60. **Hancock CR**, **Han D-H**, **Chen M**, **Terada S**, **Yasuda T**, **Wright DC**, **Holloszy JO.** High-fat diets cause insulin resistance despite an increase in muscle mitochondria. *Proc Natl Acad Sci USA* 105: 7815–7820, 2008. doi:10.1073/pnas.0802057105.
61. **Muoio DM.** Intramuscular triacylglycerol and insulin resistance: guilty as charged or wrongly accused? *Biochim Biophys Acta* 1801: 281–288, 2010. doi:10.1016/j.bbalip.2009.11.007.
62. **Turner N**, **Bruce CR**, **Beale SM**, **Hoehn KL**, **So T**, **Rolph MS**, **Cooney GJ.** Excess lipid availability increases mitochondrial fatty acid oxidative capacity in muscle: evidence against a role for reduced fatty acid oxidation in lipid-induced insulin resistance in rodents. *Diabetes* 56: 2085–2092, 2007. doi:10.2337/db07-0093.
63. **Wicks SE**, **Vandanmagsar B**, **Haynie KR**, **Fuller SE**, **Warfel JD**, **Stephens JM**, **Wang M**, **Han X**, **Zhang J**, **Noland RC**, **Mynatt RL.** Impaired mitochondrial fat oxidation induces adaptive remodeling of muscle metabolism. *Proc Natl Acad Sci USA* 112: E3300–E3309, 2015. doi:10.1073/pnas.1418560112.
64. **Selathurai A**, **Kowalski GM**, **Burch ML**, **Sepulveda P**, **Risis S**, **Lee-Young RS**, **Lamon S**, **Meikle PJ**, **Genders AJ**, **McGee SL**, **Watt MJ**, **Russell AP**, **Frank M**, **Jackowski S**, **Febbraio MA**, **Bruce CR.** The CDP-ethanolamine pathway regulates skeletal muscle diacylglycerol content and mitochondrial biogenesis without altering insulin sensitivity. *Cell Metab* 21: 718–730, 2015. doi:10.1016/j.cmet.2015.04.001.

65. **Seifert EL**, **Estey C**, **Xuan JY**, **Harper M-E.** Electron transport chain-dependent and -independent mechanisms of mitochondrial H_2O_2 emission during long-chain fatty acid oxidation. *J Biol Chem* 285: 5748–5758, 2010. doi:10.1074/jbc.M109.026203.
66. **Koves TR**, **Ussher JR**, **Noland RC**, **Slentz D**, **Mosedale M**, **Ilkayeva O**, **Bain J**, **Stevens R**, **Dyck JRB**, **Newgard CB**, **Lopaschuk GD**, **Muoio DM.** Mitochondrial overload and incomplete fatty acid oxidation contribute to skeletal muscle insulin resistance. *Cell Metab* 7: 45–56, 2008. doi:10.1016/j.cmet.2007.10.013.
67. **Kakimoto PAHB**, **Tamaki FK**, **Cardoso AR**, **Marana SR**, **Kowaltowski AJ.** H_2O_2 release from the very long chain acyl-CoA dehydrogenase. *Redox Biol* 4: 375–380, 2015. doi:10.1016/j.redox.2015.02.003.
68. **Rodrigues JV**, **Gomes CM.** Mechanism of superoxide and hydrogen peroxide generation by human electron-transfer flavoprotein and pathological variants. *Free Radic Biol Med* 53: 12–19, 2012. doi:10.1016/j.freeradbiomed.2012.04.016.
69. **Marinho HS**, **Real C**, **Cyrne L**, **Soares H**, **Antunes F.** Hydrogen peroxide sensing, signaling and regulation of transcription factors. *Redox Biol* 2: 535–562, 2014. doi:10.1016/j.redox.2014.02.006.
70. **Jang HH**, **Lee KO**, **Chi YH**, **Jung BG**, **Park SK**, **Park JH**, **Lee JR**, **Lee SS**, **Moon JC**, **Yun JW**, **Choi YO**, **Kim WY**, **Kang JS**, **Cheong G-W**, **Yun D-J**, **Rhee SG**, **Cho MJ**, **Lee SY.** Two enzymes in one: two yeast peroxiredoxins display oxidative stress-dependent switching from a peroxidase to a molecular chaperone function. *Cell* 117: 625–635, 2004. doi:10.1016/j.cell.2004.05.002.
71. **Smith CD**, **Schmidt CA**, **Lin C-T**, **Fisher-Wellman KH**, **Neufer PD.** Flux through mitochondrial redox circuits linked to nicotinamide nucleotide transhydrogenase generates counterbalance changes in energy expenditure. *J Biol Chem* 295: 16207–16216, 2020. doi:10.1074/jbc.RA120.013899.
72. **Brand MD.** Mitochondrial generation of superoxide and hydrogen peroxide as the source of mitochondrial redox signaling. *Free Radic Biol Med* 100: 14–31, 2016. doi:10.1016/j.freeradbiomed.2016.04.001.